Competing antiferromagnetic and spin-glass phases in a hollandite structure

Y. Crespo,[1,*] A. Andreanov,[1,2] and N. Seriani[1]

[1]*The Abdus Salam ICTP, Strada Costiera 11, I-34151 Trieste, Italy*
[2]*Max-Planck-Institut für Physik komplexer Systeme, Nöthnitzer Strasse 38, 01187 Dresden, Germany*

We introduce a simple lattice model with Ising spins as a zeroth-order approximation of the hollandite-type magnetic compounds. We argue that geometrical frustration of the lattice in combination with nearest-neighbor antiferromagnetic (AFM) interactions are responsible for the appearance of a spin-glass phase in presence of disorder. We investigate this system numerically using parallel tempering. The model reproduces magnetic transitions present in some oxides with hollandite structure and displays a rich phenomenology: in the absence of disorder we have identified five different ground states, depending on the relative strength and sign of the interactions: one ferromagnetically ordered, three antiferromagnetically ordered, and one disordered, macroscopically degenerate ground state. Remarkably, for the sets of AFM couplings having an AFM ground state in the clean system, there exists a critical value of the disorder above which the ground state becomes a spin glass while maintaining all the couplings antiferromagnetically. This model presents this kind of transition with nearest-neighbor frustrated AFM interactions. We argue that this model is useful for understanding the relation between AFM coupling, disorder, and appearance of spin-glass phases.

I. INTRODUCTION

Spin glasses are magnetic phases where disorder and frustration suppress any simple ordered patterns, like ferro- or antiferromagnetic states, and have instead a spin-freezing transition into an amorphous *glassy* ordered state at low temperature (or other control parameters). Such glassy states feature many interesting and unusual properties,[1] like power-law correlations in the absence of any broken symmetry[2] and nontrivial long-time behavior. The free-energy landscape of such systems is very rough and has many metastable states that are separated by high barriers.[3]

Two crucial ingredients necessary to produce a spin glass are disorder and frustration. The canonical representatives of spin glasses, magnetic alloys, have an oscillating long-range Ruderman-Kittel-Kasuya-Yosida (RKKY) spin-spin interaction.[4] The standard Edwards-Anderson model[5] has quenched random nearest-neighbor couplings of both signs which mimics the frustrating effect of the longer-ranged RKKY interaction. In both cases, as well as in many others, it is the interaction, which is both disordered and frustrating [i.e., a mixture of ferromagnetic (FM) and antiferromagnetic (AFM) couplings], that is responsible for the appearance of a spin glass. There is also a large class of materials where frustration has geometrical origin: the combination of the AFM interactions and geometry of the lattice suppresses the natural AFM order[6] and makes the system extremely susceptible to perturbations.[6] In this case often even a small disorder in the coupling strengths, that does not change their AFM character, is enough to obtain a spin-glass.[7–9] Consider now a geometrical frustrated system with nearest-neighbor AFM couplings of different strengths. Can the AFM ground state still survive? If so, is it possible to obtain a spin-glass phase by tuning the disorder and maintaining the AFM interactions? How much disorder is needed to break the AFM ground state?

In this paper we introduce a model which addresses these points and extends the previously studied models of spin-glass transition in the presence of geometrical frustration. In the absence of disorder in the couplings, we have identified five main types of ground states: one FM ordered, three AFM ordered, and one disordered, macroscopically degenerate ground state. From the theoretical point of view it is interesting to study the transition from an AFM ground state to a spin-glass phase by increasing disorder in a system containing only nearest-neighbor AFM couplings. Remarkably, despite the geometrical frustration, the natural AFM order is not always suppressed by introducing disorder and a critical amount is required to introduce a spin-glass phase. This provides an example of a system where the geometry forces different ground states to compete and there is a direct transition from an AFM state to a spin-glass phase by tuning the disorder, while maintaining AFM couplings only. This model presents this kind of transition with nearest-neighbor frustrated AFM interactions. In other models such transition becomes possible if longer ranged interactions are allowed.[9]

This model is inspired by manganese oxides compounds (MnO$_2$) with the hollandite structure, such as α-MnO$_2$,[10,11] K$_{1.5}$(H$_3$O)$_x$Mn$_8$O$_{16}$,[12] Ba$_{1.2}$Mn$_8$O$_{16}$,[13] etc. Experimentally these materials have a rich magnetic phenomenology[12,14–17] whose origin is poorly understood. In particular it is not clear whether the magnetic properties can be explained by considering only bulk properties, like the effects of doping and frustration, or whether surface effects have to be taken into account as well. Therefore a theoretical description of these materials is needed for a better understanding of their magnetic behavior. This will open the venue for a systematic approach to tune and optimize the properties of these compounds. The simple model presented here is a first step in this direction.

Hollandite-type Mn oxides are nanoporous materials[10,11] that are interesting on their own for their large number of applications, as ionic conductor, as catalysts for oxygen reduction and oxygen evolution reactions, in lithium-air batteries,[18–20] in supercapacitors,[21] for the energy extraction from salinity differences,[22] and as a water oxidation catalyst.[23]

The large lateral size of the channels [see Fig. 1(a)], of the order of 0.46 nm, makes it possible for some big cations such as K^+, Na^+, Ba^{2+}, and H_3O^+ to be introduced during material synthesis,[12–15,24] thus opening the possibility to tune the magnetic, chemical, and physical properties by cation doping. The magnetic nature of this compound originates from the presence of the manganese ions, which have localized magnetic moments due to the open shell of d electronic states.[12,24,25] These properties, together with the magnetic frustration due to the structural triangles [see Fig. 1(c)], are at the origin of the rich variety of magnetic ordered phases that have been identified experimentally in these materials.

For example, α-MnO_2 in the absence of doping elements in the channels, i.e., in the absence of disorder, has an AFM phase at low temperatures (T).[16,17] Luo *et al.* have investigated the dependence of the magnetic phase on the doping of potassium ions,[14,15] and have shown that above a critical concentration of K^+ ions, a difference in the magnetic susceptibilities between zero-field-cooled and field-cooled samples is observed which is interpreted as the onset of the spin-glass phase. When all the sites available for K insertion became full, the AFM behavior was recovered. The spin-glass phase was previously observed in the case of the KMn_8O_{16} material[11] with the same behavior of the magnetic susceptibilities. Lan and co-workers proposed a surface effect to be responsible for the spin-glass behavior in sodium-doped α-MnO_2 nanorods.[17] They proposed that, at low temperatures, the bulk of the system is in an AFM state while the surface spins contribute to a net magnetic moment of the specimen.[17] Their explanation thus relies on the high surface area present in the nanostructured material rather than on the doping.

Due to the complicated structure of these materials, it is important, as a starting point, to disentangle the contributions of bulk effects (doping and frustration) and surface effects, in order to gain a better understanding of the magnetic properties of these compounds. In this paper we study a simple model based on Ising spins. Our aim is to identify mechanisms that create spin-glass phases in this class of materials, i.e., manganites. The Ising spins are more convenient for this purpose: identifying a spin glass in a model with vector spins is a much more challenging problem. Therefore we

decided to analyze the Ising model first, since, if the spin-glass transition is not present in the Ising case, there is definitely no spin-glass phase for vector spins. Another motivation to study the Ising model is the fact that even such a simple model features a rich phase diagram, which is of interest in its own right. Its study suggests a new way to closely investigate the role and importance of frustration and disorder for the emergence of spin-glass phases. Additionally, this model is able to reproduce essential features of manganese oxides, i.e., an AFM ground state in the clean case, transition to a spin-glass phase at increasing disorder, and the need of a critical amount of disorder for this transition to occur.[14] At the same time, this model is a crude approximation to manganese oxides, which are known to be Heisenberg magnets with weak exchange anisotropy.[26–28] Consequently, our model cannot capture realistic low-T magnetic configurations of manganites, like noncollinear AFM or helical magnetic ground states, that were identified in some compounds.[12,25] Summarizing, we consider this model as a zeroth-order approximation towards more realistic models that describe magnetic properties of materials with hollanditelike lattice structures.

The paper is organized as follows: We introduce the model in Sec. II and study its properties in the clean limit in Sec. III. Next we discuss the mechanism which generates a spin-glass phase in the doped samples and present numerical results in support the mechanism in Sec. IV. Conclusions are given at the end.

II. MODEL

The materials that inspired this study have a complicated lattice structure known as the hollandite lattice. This structure consists of two octahedra joined at the edges to form the wall of (2×2) channels (see Fig. 1), and belongs to a family of crystals which differ from each other only by the lateral size of the channels, like ramsdellite (1×2), romanechite (2×3) and todorokite (3×3).[10,29–32] In the case of manganese oxides each octahedron is formed by a MnO_6 unit.

The magnetism is due to the interaction of the magnetic moments localized on the manganese ions, which interact with each other through oxygen-mediated superexchange.[12,13,24,33,34] We consider the simplest possible model compatible with the lattice structure and place classical Ising spins on Mn sites of the hollandite lattice. The choice of the Ising spins is mainly dictated by simplicity. The real manganese oxides do not have a strong Ising anisotropy and are better described by Heisenberg spins. However for our purposes, i.e., identifying a possible mechanism that leads to spin-glass phase, the Ising spins are more convenient. Simulating vector spins glass is a much more difficult problem and, even when the spin-glass phase is identified in simulations, its nature is still debated.[35,36] Therefore it is better to simulate first the Ising model since, if the spin-glass transition is not present in this case, there is definitely no spin-glass phase for the vector spins. Another reason for studying the Ising model is the fact that even this case has a phase diagram which is interesting in its own right.

We get a lattice of spins which has eight spins per unit cell as shown in Fig. 1. We consider nearest-neighbor interactions
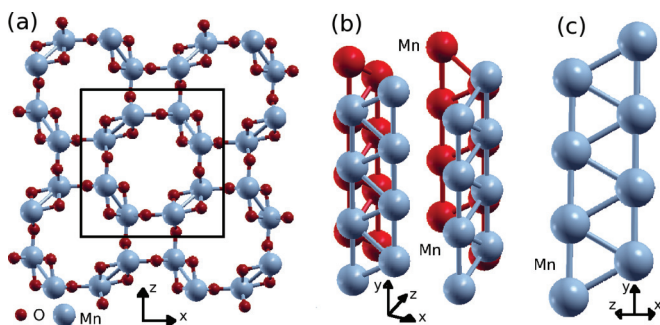

FIG. 1. (Color online) Different views of the hollandite structure for the case of α-MnO_2 compound (Refs. 14 and 15): (a) the XZ plane containing both Mn and oxygen (O) atoms; (b) panoramic view of the channel with only Mn atoms; (c) structural triangles composed by magnetic atoms that play an important role in setting the magnetic properties of the oxide.
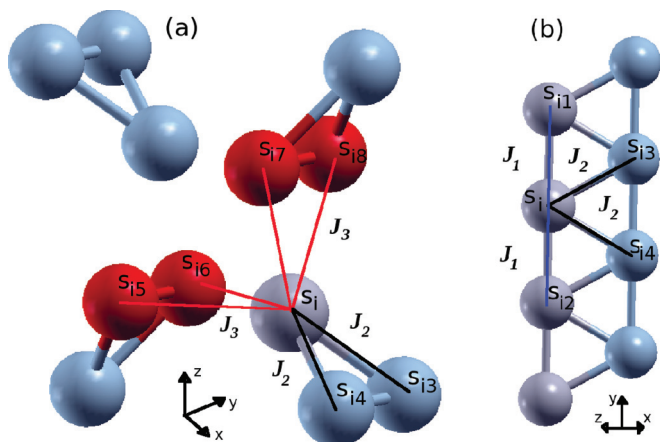
FIG. 2. (Color online) The graphical representation of the Hamiltonian (1). Links of different color represent the three couplings J_1 (blue), J_2 (black), and J_3 (red).

and the Hamiltonian reads

$$\mathcal{H} = \sum_{\langle ij \rangle_1} J_1^{ij} s_i s_j + \sum_{\langle ij \rangle_2} J_2^{ij} s_i s_j + \sum_{\langle ij \rangle_3} J_3^{ij} s_i s_j, \quad (1)$$

where $\langle ij \rangle_k$ denotes three different groups of nearest neighbors of a spin i. The partitioning of the neighbors and the corresponding couplings J_1, J_2, J_3 are detailed in Fig. 2. Such division and the choice of three different coupling constants are dictated by the structure of the material: all these three classes of nearest neighbors are quite close to the atom i: the distance to atoms of the first group is $\sim$2.86 Å, while the atoms of the second and third groups are at distances of 2.91 and 3.44 Å, respectively.

Despite the simplicity of the Hamiltonian (1) it admits many different ordered magnetic ground states depending on relative strengths and signs of the couplings J_k for $k = 1,2,3$. This richness reflects the complicated geometry of the hollandite lattice. There is no experimental insight for the selection of particular values of the couplings J_k, $k = 1,2,3$ and in general we expect them to be system dependent. Since in hollandite-type structures the angles of Mn-O-Mn bridges take values between 80° and 130°, simple symmetry rules to determine the sign of the magnetic couplings such as the Goodenough-Kanamori rules[13,33,34] cannot be straightforwardly applied. As the undoped compound is known experimentally to have an AFM ordering,[16] we omit the case of all the FM couplings, since in this case the phase diagram consists only of paramagnetic and FM phases. We focus instead on the simplest assumption, namely that the first nearest neighbor coupling is AFM ($J_1 > 0$), and then study the phases that appear in the J_2/J_1 vs J_3/J_1 plane. The case $J_1 < 0$ is also mentioned. As we are interested in the study of the transition to the spin-glass phase at increasing disorder, we start in the region of the phase space where $J_2 > 0$ and $J_3 > 0$. Such choice of the couplings is interesting from the theoretical point of view because it gives the transition from an AFM ground state to a spin-glass phase in a system containing only nearest-neighbor AFM couplings.

III. CLEAN SYSTEM

We start by studying the clean limit where the strengths of all the couplings J_k $k = 1,2,3$ are constants and do not fluctuate in space (no disorder). Experiments indicate a transition to an AFM phase[16] at low enough temperatures. For this reason we take the first-nearest-neighbor coupling J_1 positive: $J_1 > 0$. In order to discover all the possible ground states of the Hamiltonian (1) in this case we proceed by trying to minimize every term of the Hamiltonian.

As shown in Fig. 2, every Mn atom s_i interacts with eight other Mn atoms $s_{ik}, k = 1, \ldots, 8$. The total energy (E_T) can then be written as a sum of local energies of each site (E_i): $E_T = \sum_i E_i/2$ where

$$E_i = s_i[J_1(s_{i1} + s_{i2}) + J_2(s_{i3} + s_{i4})$$
$$+ J_3(s_{i5} + s_{i6} + s_{i7} + s_{i8})]. \quad (2)$$

Let us suppose now that $J_2 > 0$ is the strongest interaction in the lattice, then to minimize the interaction of s_i with the second group of nearest neighbors we select $s_{i3} = s_{i4} = -s_i$ for all sites i. This selection has two effects: (i) it creates a FM order along all the chains of Mn atoms in the y direction, and (ii) it imposes that the chains connected by J_2 [see Fig. 2(b)] are coupled antiferromagnetically, nevertheless it leaves the J_3 connections "free." Therefore we have $s_{i1} = s_{i2} = s_i$ and $s_{i5} = s_{i6}$, $s_{i7} = s_{i8}$ (see Fig. 2). Notice now that this spin configuration allows us to minimize at the same time the interaction with the third group of nearest neighbors, the precise configuration depending on the sign of J_3. If we have $J_3 > 0$, then we select $s_{i5} = s_{i6} = -s_i$ and $s_{i7} = s_{i8} = -s_i$, obtaining that the minimal configuration will have a total energy per spin given by $E_T = J_1 - J_2 - 2J_3$ and spins ordered in a C-type AFM (C-AFM) state. The C-AFM order is composed of FM chains which are coupled antiferromagnetically[37,38] as shown in Fig. 3(a). In the case of $J_3 < 0$ we must set $s_{i5} = s_{i6} = s_i$ and $s_{i7} = s_{i8} = s_i$ and the spins will be ordered in a single configuration that we call $A2$-AFM state, as shown in Fig. 3(b). The total energy of this configuration is $E_T = J_1 - J_2 + 2J_3$. The A-type AFM configuration consists of FM planes coupled antiferromagnetically,[37] in this particular case we obtain a set of two FM planes. This set is then coupled antiferromagnetically [see Fig. 3(b)] and this is the reason we refer to it as $A2$-AFM.

If we assume $J_2 < 0$ as the strongest interaction in the lattice, then the interaction is minimized by selecting $s_{i3} = s_{i4} = s_i$ for all sites i. Again we create a FM order along all the chains of Mn atoms in the y direction but now it imposes that the chains connected by J_2 [see Fig. 2(b)] are coupled ferromagnetically while the J_3 connections are still free. So we can make the same reasoning as in the previous case. Therefore if $J_3 < 0$ the configuration that minimizes the energy is a FM configuration with energy $E_T = J_1 + J_2 + 2J_3$ and if $J_3 > 0$ we obtain a unique configuration with energy $E_T = J_1 + J_2 - 2J_3$ that we have called $C2$-AFM, because it is composed of two FM lines coupled antiferromagnetically as shown in Fig. 3(c). The total energy per spin of the minimal configuration for each case can be obtained by using the equation
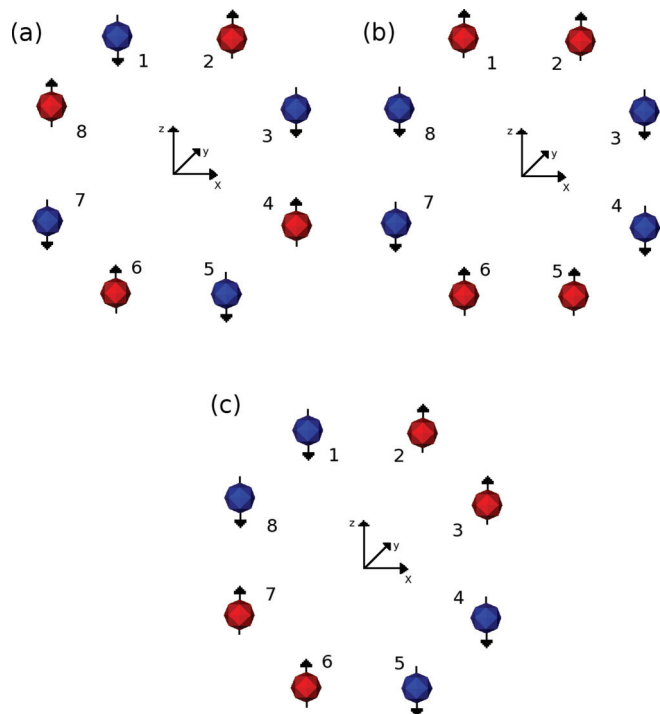
$$E_T = J_1 - |J_2 + 2J_3|. \quad (3)$$

FIG. 3. (Color online) Configuration of three possible AFM ground states on the hollandite lattice at $T = 0$, $J_1 > 0$, and $2J_1 < |J_2 + 2J_3|$. (a) C-type antiferromagnetic (C-AFM), for $J_2 > 0$ and $J_3 > 0$ there is an AFM alignment in the clockwise/counterclockwise direction. (b) $A2$-AFM, for $J_2 > 0$ and $J_3 < 0$, composed of sets of two FM planes, the sets are then coupled antiferromagnetically between them. (c) $C2$-AFM, for $J_2 < 0$ and $J_3 > 0$, composed of two FM lines coupled antiferromagnetically.

Finally let us suppose that J_1 is the strongest coupling, then, to minimize the energy, we must impose that $s_{i1} = s_{i2} = -s_i$ for each site i. This selection creates an AFM order along all the chains of Mn atoms in the y direction (see Fig. 2). As a consequence we will have that $s_{i3} = -s_{i4}$, $s_{i5} = -s_{i6}$, $s_{i7} = -s_{i8}$ and the total energy per spin is

$$E_T = -J_1. \tag{4}$$

Notice that in this approximation the strength and signs of J_2 and J_3 are irrelevant, as the interaction of S_i with the second and third groups of nearest neighbors cancels out exactly. To summarize this picture, one can think that the configurations that minimize the J_1 interaction are composed by a collection of one-dimensional Mn-Mn chains, each having AFM order of spins. However the chains are completely uncorrelated between them and arranged in such a way as to form the channels of the hollandite structure [see Fig. 6(a)]; for this reason we have called this phase a "correlated geometrically frustrated phase" (corr-GFP). That is, there is a perfect AFM order in the y direction, but no order in the transverse direction. If we consider a single unit cell replicated in the y direction then we will have 2^8 possible configurations with the same energy per spin $E_T = -J_1$. Since each chain is completely uncorrelated to the others, for an increasing number of cells in the x and z directions, N_{cell}^{xz}, the number of ground states is

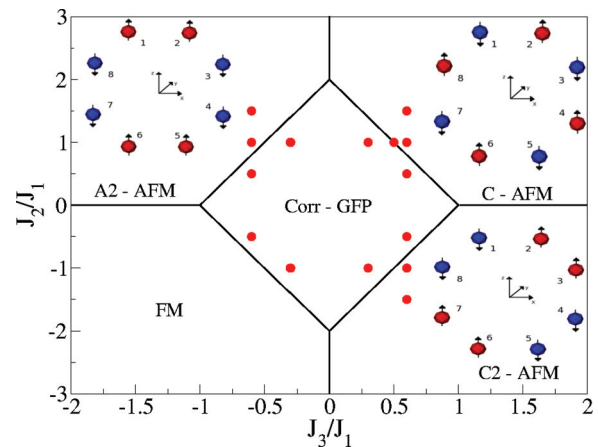FIG. 4. (Color online) Phase diagram of the Hamiltonian (1) for $J_1 > 0$; five different phases are observed: three AFM (C-AFM, $A2$-AFM, $C2$-AFM), one FM, and one geometrically frustrated (corr-GFP) with perfect anticorrelation along the y axes [see Fig. 6(a)]. Also geometrically frustrated phases with zero area are found at every boundary between any of the five phases. Filled circles represent the points in the phases diagram probed via the Monte Carlo simulations.

growing as $2^{8N_{cell}^{xz}}$, i.e., the ground state is macroscopically degenerate. This choice of couplings gives the maximum frustration.

To complete the picture of the phase diagram for $J_1 > 0$ for a given point (J_2/J_1, J_3/J_1) we notice from Eqs. (3) and (4) that only three cases are possible. In the first case $2 > |J_2/J_1 + 2J_3/J_1|$ we have the corr-GFP as the ground state. In the second case $2 < |J_2/J_1 + 2J_3/J_1|$ we have the following four possible ground states: (i) C-AFM for $J_2 > 0$ and $J_3 > 0$, (ii) $A2$-AFM for $J_2 > 0$ and $J_3 < 0$, (iii) $C2$-AFM for $J_2 < 0$ and $J_3 > 0$, and (iv) FM for $J_2 < 0$ and $J_3 < 0$ (see Fig. 4). The third case $2 = |J_2/J_1 + 2J_3/J_1|$ defines the phase boundary and has the form of a rhombus centered at the origin and with the bigger diagonal along the J_2/J_1 axis. At the boundaries the magnetic properties of the model are different: the ground state is exponentially degenerate since any two of the ground states discussed above have equal energies and can be mixed freely. Therefore there is no order down to zero temperature and the AFM alignment along the y direction is suppressed. We believe that this lends support to the view that the system might be in a classical spin liquid phase.

We have checked the validity of the above arguments by performing Monte Carlo simulations[39] of a clean system with $N = 2048$ Ising spins and a simulation cell of volume $V = 256V_0$ where V_0 is the volume of the unit cell composed by eight spins. We used periodic boundary conditions. The standard Metropolis[39] rule with single spin-flip updates was used. The points of the phase space where we have checked our arguments with the Monte Carlo simulations are plotted in Fig. 4 as red circles. To study and confirm the transitions from a paramagnetic phase to one of the AFM ground states we computed the appropriately defined staggered magnetizations
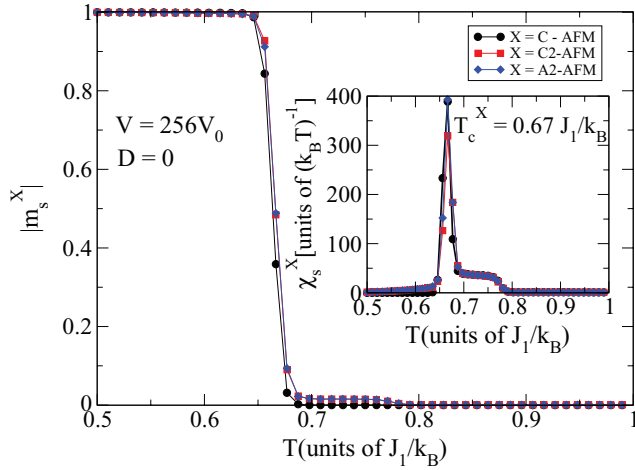
FIG. 5. (Color online) Staggered magnetizations m_s^X, for each AFM ground state X as defined in Eq. (5), as a function of temperature for the clean system ($D = 0$), $N = 2048$ spins, volume $V = 256V_0$, where V_0 is the volume of the unit cell. The couplings are equal to $J_1 = 1$ for all cases, $J_2/J_1 = 1$ and $J_3/J_1 = 0.6$ for $X = C$-AFM, $J_2/J_1 = 1$ and $J_3/J_1 = -0.6$ for $X = A2$-AFM, and $J_2/J_1 = -1$ and $J_3/J_1 = 0.6$ for $X = C2$-AFM. Inset: the staggered susceptibility χ_s^X as a function of temperature. The sharp peak signalizes the transition from the paramagnetic phase to one of the AFM orders.

$$m_s^X = M_s^X/N:$$

$$M_s^{C\text{-}AFM} = \sum_{i=1}^{N} (-1)^i s_i,$$

$$M_s^{A2\text{-}AFM} = \sum_{i=1}^{N} f_{A2}(i) s_i, \tag{5}$$

$$M_s^{C2\text{-}AFM} = \sum_{i=1}^{N} f_{C2}(i) s_i,$$

where the site index i is selected in the clockwise direction inside the unit cell as shown in Fig. 3 (i_{1-8}), X refer to each AFM ground state $X =$(C-AFM, $A2$-AFM, $C2$-AFM),

$$f_{A2}(i) = \begin{cases} 1 & \text{if } i = 1 + 4n \quad \text{or} \quad i = 2 + 4n, \\ -1 & \text{if } i = 3 + 4n \quad \text{or} \quad i = 4 + 4n, \end{cases} \tag{6}$$

$$f_{C2}(i) = \begin{cases} 1 & \text{if } i = 1 + 4n \quad \text{or} \quad i = 4 + 4n, \\ -1 & \text{if } i = 2 + 4n \quad \text{or} \quad i = 3 + 4n, \end{cases} \tag{7}$$

and $n = 0, 1, 2, \ldots$. The points ($J_2/J_1, J_3/J_1$) in phase space selected for the calculations are (1,0.6), (1,−0.6), and (−1,0.6) with $J_1 = 1$. The temperature dependence of m_s^X computed using Monte Carlo simulation is shown in Fig. 5. In all cases $m_s^X = 0$ for high temperatures and $m_s^X \to 1$ for temperatures close to zero, indicating an AFM order. We also computed the staggered susceptibilities,

$$\chi_s^X = \left. \frac{dm_s}{dh_s} \right|_{h_s=0} = \left(\langle (M_s^X)^2 \rangle - \langle M_s^X \rangle^2 \right)/k_B T,$$

where k_B is the Boltzmann constant and T the temperature. As shown in the inset of Fig. 5, the staggered susceptibility has a sharp peak at the same temperature where m_s^X becomes nonzero. Curiously, the critical temperature $T_c^X = 0.67 J/k_B$

estimated from the divergence of χ_s^X (see the inset of Fig. 5) is the same in all the AFM phases. This fact is related with the choice of symmetric points in the phase space, for which the ground-state energy is the same in all three cases (but not the ground states themselves).

We have also done a calculation inside the corr-GFP at the point ($J_2/J_1 = 0.3, J_3/J_1 = 0.6$). The Monte Carlo results confirm the picture for the case $2 > |J_2/J_1 + 2J_3/J_1|$. The staggered magnetizations are always zero and the staggered susceptibilities do not display any sharp features down to $T = 0$. Such behavior is typical for systems where the combination of lattice geometry and interactions suppresses the natural AFM order. At low temperatures, instead, they enter a phase known as collective paramagnet[6] with power-law/exponential correlations depending on the structural properties of the lattice (bipartite/nonbipartite). We have computed the spin-spin correlation functions along different axes of the unit cell as shown in Fig. 6(b). Unlike other geometrically frustrated systems, there is a clear AFM alignment of spins along the y direction and a fast exponential decay as we deviate from this direction (x,z,xy,xz,yz,xyz). Also the eight spins of the unit cell are uncorrelated as illustrated in Fig. 6. This confirms the picture developed above, based on a simple energy minimization argument.

To conclude, we look at the case $J_1 < 0$. Following the same minimization argument, it is easy to convince yourself that one can always minimize simultaneously every term in the Hamiltonian (1), implying that the system is not frustrated in this case. Thus the corr-GFP phase disappears and only the nondegenerate ground states survive. This case is less interesting than the previous case ($J_1 > 0$) and it does not display any new physics.

IV. DISORDERED SYSTEM

We now turn to the disordered case and study what effect the disorder has on the physical properties of the system described by the Hamiltonian (1). Usually spin-glass behavior is associated with the presence of disorder and frustration in the system.[40] As discussed above, the clean system has geometrical frustration (for $J_1 > 0$). We suggest the following mechanism to explain the appearance of the spin-glass phase in the experimental results: as the dopant ions penetrate into the channels of the hollandite structure,[24] they locally modify the compound and therefore also the magnetic interactions between the spins, i.e., they generate fluctuations in the AFM couplings J_k, $k = 1, 2, 3$. In principle, this could happen through different mechanisms, such as doping-induced strain or changes in the local electronic structure through charge donation. When the dopant penetrates into the channels it could induce local strains in the lattice. The strains generate random quenched fluctuations in AFM couplings J_k through the magnetoelastic coupling. This is a well-known mechanism that causes spin-glass transition in many geometrically frustrated systems.[7,8] On the other hand, charge donated by the doping elements modifies the oxidation state of manganese, producing a local mixture of Mn^{+3} and Mn^{+4}.[10,14,41] This local change in the electronic properties induces fluctuations in the strength of magnetic spin-spin interaction, breaking the symmetry of the system (all Mn atoms are equivalent in the clean case).
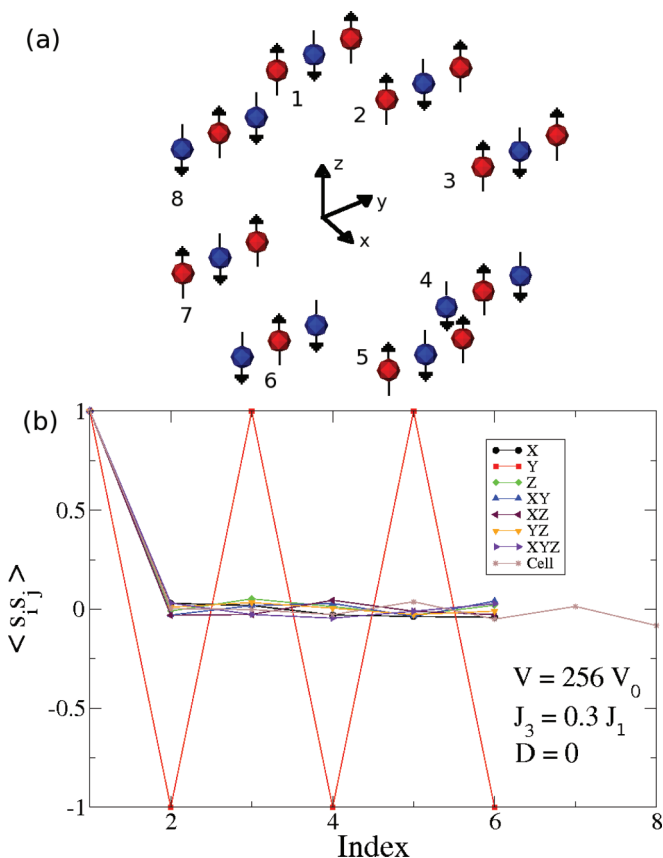
(a)

(b)

FIG. 6. (Color online) (a) Single unit cell replicated in the y direction. The spin configuration corresponds to one of the possible ground states with energy per spin $E_T = -J_1$ ($J_1 > 0$ is the strongest coupling). The spins are always aligned antiferromagnetically in the y direction for these ground states, while there is no order in the perpendicular direction. (b) The spin-spin correlations in the geometrically frustrated phase for the x, y, z, xy, xz, yz, xyz directions and inside the unit cell. Here the index is defined as the number of times you have to move in each direction to find s_j, e.g., in the xy direction index $= 2$ means that s_j is located at a distance of $\sqrt{(2L_x)^2 + (2L_y)^2}$ where L_x and L_y are the length of the unit cell in the x and y direction, respectively. In the case of "cell" the index runs over the eight atoms of the unit cell.

Estimating the variations in the AFM couplings depends on which of the previous two mechanisms dominates the magnetic interaction and therefore on the particular system in consideration. In our model we mimic these fluctuations by introducing continuous disorder in the couplings J_k. A discrete distribution of the couplings would be a more accurate model for some systems, for example a system where the doping-induced strain is not present. Nevertheless, the difference between the continuous and discrete disorder is *irrelevant* for the spin-glass transition, since universality of the glass transition with respect to the continuous vs discrete nature of the disorder is well established.[42] This justifies our usage of the continuous disorder. In this paper we focus on the case where all the couplings remain AFM in order to study the possibility and details of the C-AFM to spin-glass transition. We assume fluctuations of the couplings J_k around their clean values so that the couplings remain AFM. The presence of quenched

fluctuations in the couplings J_k is crucial for the appearance of the spin-glass phase.[7–9]

Since we want to study the transition between the C-AFM ground state and the spin-glass phase we start in the $J_2/J_1 + 2J_3/J_1 > 2$ part of the phase diagram of our model. We propose the following mechanism for the appearance of the spin glass in the model: randomness in the AFM couplings $J_k, k = 1 \ldots 3$, produces local regions of the lattice where the condition $J_2/J_1 + 2J_3/J_1 > 2$ is violated and that local patch has the C-AFM ordering locally disfavored. The presence of such patches frustrates the system, and generates the spin-glass phase. Such mechanism implies that the spin glass can only appear for sufficiently strong fluctuations in the strengths of the couplings, since one has to violate the condition $J_2/J_1 + 2J_3/J_1 > 2$. Therefore we expect the critical strength of the disorder to be an increasing function of the distance to the point $J_2/J_1 + 2J_3/J_1 = 2$. Since the amount of disorder depends on the doping, we need a sufficiently large doping to produce the spin glass. This is exactly what is seen in experiments: Luo and co-workers[14,15] have found that a critical amount of K^+ doping in α-$K_x MnO_2$ is needed to see the spin-glass phase.

We have performed numerical simulations of the model with disorder to confirm our ideas. The AFM couplings $J_{ij} = J_{ji} = J_k + \Delta$ are different for each link connecting a pair of atoms $i, j = 1 \ldots N$. The disorder Δ is drawn from the box distribution $-D < \Delta < D$ where D sets the scale for the strength of the quenched fluctuations. Glassy systems are notoriously difficult to simulate at low temperatures and we used parallel tempering[43–45] to equilibrate the samples at low temperatures. We used up to $N_s = 200$ samples to compute the disorder average. In every case we have tested that convergence to the average was achieved.

We first show the results for amounts of disorder ($D < J_2/J_1 + 2J_3/J_1 - 2$) where the C-AFM phase is still present. In Fig. 7 we show the plot of the staggered magnetization vs temperature for $D = 0.18J_1$. The parameters of the system are the same as those of the clean case ($D = 0$; see Fig. 3):
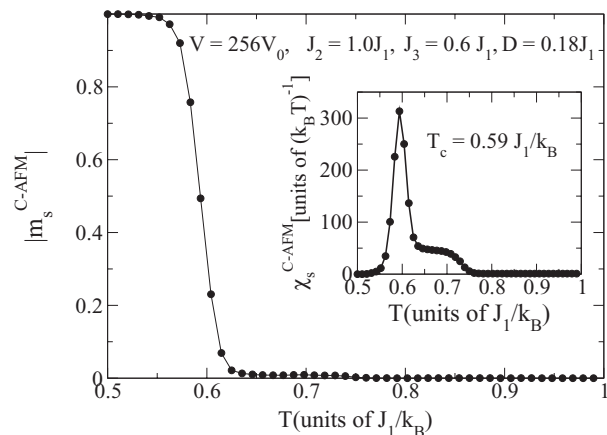

FIG. 7. Staggered magnetisation m_s^{C-AFM} as a function of temperature for the same system as in Fig. 5, except now disorder $D = 0.18J$, drawn from the box distribution, is present in the AFM couplings. Clearly, this disorder strength is not enough to destroy the C-AFM phase. Inset: staggered susceptibility χ_s^{C-AFM} as a function of temperature for the same system and the same disorder strength.

$J_1 = J_2 = 1$ and $J_3 = 0.6J_1$, $N = 2048$ spins, $V = 256V_0$ where V_0 is the volume of the unit cell. We see that this amount of disorder is not enough to destroy the C-AFM phase but the critical temperature $T_c = 0.59J/k_B$ extracted from the position of the sharp peak of the staggered susceptibility (see Fig. 7) is reduced in comparison with the clean case where $T_c = 0.67J_1/k_B$.

Upon further increase of the strength of the disorder the C-AFM phase is completely suppressed at $D = 0.4J_1$ and the spin-glass phase appears instead at low temperatures. To characterize the paramagnetic to spin-glass transition we have studied the Binder cumulant[46,47] which is defined as

$$G = \frac{1}{2}\left[3 - \frac{\overline{\langle q^4 \rangle}}{\overline{\langle q^2 \rangle}^2} \right], \qquad (8)$$

where $\langle \cdots \rangle$ is the thermal average and $\overline{\cdots}$ is the average over the disorder; q is the overlap between two independent replicas of the system (s_i^1, s_i^2) with the same realization of disorder:

$$q = \frac{1}{N}\sum_{i=1}^{N} s_i^1 s_i^2. $$

The Binder cumulant G is a dimensionless parameter that goes to zero for high temperatures and it is of order 1 in the spin-glass phase and has the following finite-size scaling[47] close to the transition:

$$G = g[V^{1/3\nu}(T - T_c)], \qquad (9)$$

where V is the volume of the sample and T_c is the critical temperature. These properties make the Binder parameter G a useful tool to study spin-glass phase transitions and it has been widely used for this purpose,[10,48–50] as all curves of G generated for different system sizes will intersect at T_c. As a complementary parameter we have also computed the overlap distribution $P(q)$ that has the finite-size scaling form:[47]

$$P(q) = V^{\beta/3\nu} p(q)[q V^{\beta/3\nu}, V^{1/3\nu}(T - T_c)], \qquad (10)$$

where ν and β are the critical exponents which are obtained by fitting the data for different system sizes to a single master curve.

The parallel tempering simulations were performed for systems with AFM couplings $J_1 = J_2 = 1$, $J_3 = 0.6J_1$ and disorder $D = 0.4J_1$. The system sizes are $V = 54V_0$, $V = 96V_0$, $V = 150V_0$, $V = 256V_0$. In all four cases the C-AFM phase was suppressed in favor of a spin-glass phase. The inset of Fig. 8 shows the Binder cumulant as a function of temperature for the four system sizes. There is a clear crossing of the Binder cumulant curves indicating the spin-glass transition near $T_c = 1.19J_1/k_B$ for $D = 0.4J_1$.

Using this estimate for T_c we collapsed all the data onto a single master curve according to Eq. (9) as shown in Fig. 8 with the critical exponent $\nu = 0.86$. We have also studied the overlap distribution $P(q)$ for the four system sizes at the temperature $T = 1.20J_1/k_B$, close to the critical temperature $T_c = 1.19J_1/k_B$ (see Fig. 9). Rescaling the $P(q)$ curves for different system sizes according to Eq. (10), a good collapse on a master curve is obtained for the ratio of the critical exponents $\beta/\nu = 0.42$ from which we get $\beta = 0.36$.

The values $\beta = 0.36$ and $\nu = 0.86$ are very different from the conventional values of the critical exponents for
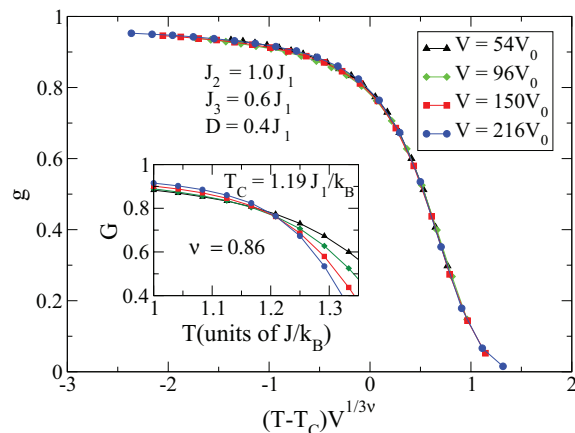

FIG. 8. (Color online) Scaled Binder cumulant as defined in Eq. (9) for four system sizes $V = 54V_0$, $V = 96V_0$, $V = 150V_0$, $V = 256V_0$ where V_0 is the volume of the unit cell, the interactions $J_1 = J_2 = 1$ and $J_3 = 0.6J_1$ were considered with a disorder of $D = 0.4J_1$. Inset: Binder cumulant as defined in Eq. (8) as a function of temperature.

the spin-glass transition in $d = 3$: $\beta = 0.77(5)$, $\nu = 2.45(15)$ (see Ref. 42 and references therein). Since these exponents are known to be hard to evaluate precisely due to large finite-size effects in spin glasses[42] and the absence of any good reason which could change the exponents from their conventional values, we attribute the discrepancy to the fact that the system sizes studied are too small. We found that the critical amount of disorder for obtaining the spin-glass phase for this set of parameters is $D_c = 0.28 \pm 0.02J_1$, nevertheless studying the complete phase diagram D vs J_3/J_1, D vs T and the dependence of the critical exponents on the system size requires longer simulation times and larger system sizes. However, in this paper we are focused on showing the phase diagram for the clean case and the existence of the spin-glass phase rather than on studying this transition in detail—that is the subject of a future work.
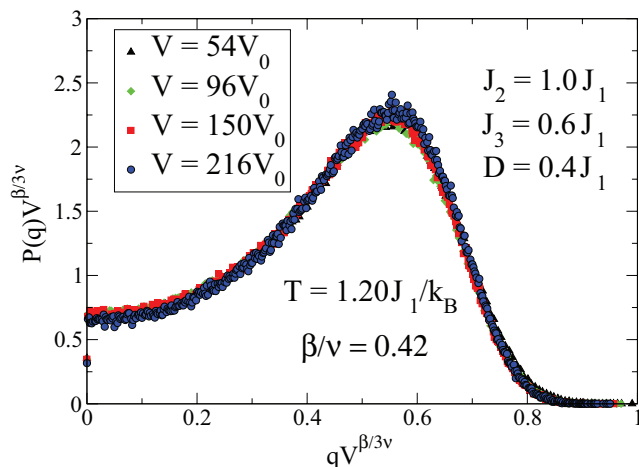

FIG. 9. (Color online) Scaling for the overlap distribution $P(q)$ at $T = 1.20J_1/k_B$ near the critical temperature $T_c = 1.19J_1/k_B$ using Eq. (10) for the same system of Fig. 8.

V. CONCLUSIONS

We have introduced a simple classical Ising spin model with nearest-neighbor antiferromagnetic (AFM) interactions and continuous disorder on a hollandite lattice. The studied system is geometrically frustrated due to the existence of structural triangles [see Fig. 1(c)] in the hollandite lattice. However, the degree of the frustration depends on the mutual values of the spin couplings. The parallel tempering Monte Carlo simulations performed for this system with clean and disordered AFM coupling strengths and different system sizes reveal that, despite the simplicity of the Hamiltonian Eq. (1) (only nearest neighbor interactions and Ising spins), it admits different phases depending on relative strengths of the AFM couplings due to the complicated geometry of the hollandite lattice. We found five different ground states in the clean case: one ferromagnetic, three AFM (see Fig. 3), and one exponentially degenerated and disordered ground state (see Fig. 6). Depending on the strengths of the interactions a small amount of disorder ($D < D_c$) in the couplings does not suppress the C-AFM order, but merely reduces the critical temperature at which the paramagnet to C-AFM transition occurs (see Fig. 7). When the disorder becomes greater than some critical value, the geometry forces different ground states to compete and there is a direct transition from the C-AFM state to a spin glass by tuning the disorder (at fixed temperature), while preserving AFM couplings. This transition was confirmed numerically by looking at the Binder cumulant (see Fig. 8). This model presents this kind of transition with nearest-neighbor AFM interactions.

Despite the fact that this model is a zeroth-order approximation of the manganese oxides, it reproduces magnetic transitions present in some oxides with hollandite crystal structure in both the clean and doped cases, i.e., an AFM ground state in the clean case, a transition to a spin-glass phase at increasing disorder, and the need of a critical amount of disorder for this transition to occur. This model shows that bulk effects (frustration and doping) are sufficient to obtain the spin glass in compounds with hollandite lattice. It would be useful to check the convergence of the critical exponents to their standard $d = 3$ values, although this requires a considerable amount of computing time. Finally, the predictive power of our model can be enhanced by studying the Heisenberg case which is more suited for the real compounds and/or by using couplings determined via *ab initio* calculations.

An interesting possible extension of our results is the study of the role and importance of frustration and disorder for emergence of spin-glass phases. The Hamiltonian (1) falls into a class of Hamiltonians, that, in the simplest case, features two distinct ordered phases depending on the value of some control parameter g. At some critical value g_c these two phases have equal energy. Disordering the interactions, i.e., the coupling g, at the critical point, puts the ordered states in competition, and it is natural to ask whether a spin-glass phase emerges, what is the universality class of the transition, and whether the transition still exists away from g_c for disorder strength above some threshold value. Answering these questions and understanding universal features of such spin-glass transitions represents an interesting open problem.

*ycrespo@ictp.it

[1] K. Binder and A. P. Young, Rev. Mod. Phys. **58**, 801 (1986).

[2] C. De Dominicis and I. Kondor, Phys. Rev. B **27**, 606 (1983).

[3] M. Mezard, G. Parisi, and M. A. Virasoro, *Spin Glass Theory and Beyond* (World Scientific, Singapore, 1987), Vol. 9.

[4] J. A. Mydosh, *Spin Glasses: An Experimental Introduction* (Taylor and Francis, London and Washington, DC, 1993).

[5] S. F. Edwards and P. W. Anderson, J. Phys. F: Metal Phys. **5**, 965 (1975).

[6] C. L. Henley, Annu. Rev. Condens. Matter Phys. **1**, 179 (2010).

[7] T. E. Saunders and J. T. Chalker, Phys. Rev. Lett. **98**, 157201 (2007).

[8] A. Andreanov, J. T. Chalker, T. E. Saunders, and D. Sherrington, Phys. Rev. B **81**, 014406 (2010).

[9] H. Shinaoka, Y. Tomita, and Y. Motome, Phys. Rev. Lett. **107**, 047204 (2011).

[10] C. P. Herrero, Eur. Phys. J. B **70**, 435 (2009).

[11] S. L. Suib and L. E. Iton, Chem. Mater. **6**, 429 (1994).

[12] H. Sato, T. Enoki, J.-I. Yamaura, and N. Yamamoto, Phys. Rev. B **59**, 12836 (1999).

[13] S. Ishiwata, J. Bos, Q. Huang, and R. Cava, J. Phys.: Condens. Matter **18**, 3745 (2006).

[14] J. Luo, H. Zhu, F. Zhang, J. Liang, G. Rao, J. Li, and Z. Du, J. Appl. Phys. **105**, 093925 (2009).

[15] J. Luo, H. Zhu, J. Liang, G. Rao, J. Li, and Z. Du, J. Phys. Chem. C **114**, 8782 (2010).

[16] N. Yamamoto, T. Endo, M. Shimada, and T. Takada, Jpn. J. Appl. Phys. **13**, 723 (1974).

[17] C. Lan, J. Gong, S. Liu, and S. Yang, Nanoscale Res. Lett. **6**, 133 (2011).

[18] P. G. Bruce, S. A. Freunberger, L. J. Hardwick, and J.-M. Tarascon, Nat. Mater. **11**, 19 (2012).

[19] G. Girishkumar, B. McCloskey, A. C. Luntz, S. Swanson, and W. Wilcke, J. Phys. Chem. Lett. **1**, 2193 (2010).

[20] M.-K. Song, S. Park, F. M. Alamgir, J. Cho, and M. Liu, Mater. Sci. Eng., R **72**, 203 (2011).

[21] G.-R. Li, Z.-P. Feng, Y.-N. Ou, D. Wu, R. Fu, and Y.-X. Tong, Langmuir **26**, 2209 (2010).

[22] F. La Mantia, M. Pasta, H. D. Deshazer, B. E. Logan, and Y. Cui, Nano Lett. **11**, 1810 (2011).

[23] V. B. R. Boppana and F. Jiao, Chem. Commun. **47**, 8973 (2011).

[24] P. Umek, A. Gloter, M. Pregelj, R. Dominko, M. Jagodič, Z. Jagličić, A. Zimina, M. Brzhezinskaya, A. Potočnik, C. Filipič, A. Levstik, and D. Arčon, J. Phys. Chem. C **113**, 14798 (2009).

[25]H. Sato, J.-I. Yamaura, T. Enoki, and N. Yamamoto, J. Alloys Compd. **262**, 443 (1997).

[26]F. Moussa, M. Hennion, J. Rodriguez-Carvajal, H. Moudden, L. Pinsard, and A. Revcolevschi, Phys. Rev. B **54**, 15149 (1996).

[27]X. Fabrèges, I. Mirebeau, S. Petit, P. Bonville, and A. A. Belik, Phys. Rev. B **84**, 054455 (2011).

[28]G. Chaboussant, A. Sieber, S. Ochsenbein, H.-U. Güdel, M. Murrie, A. Honecker, N. Fukushima, and B. Normand, Phys. Rev. B **70**, 104422 (2004).

[29]M. M. Thackeray, Prog. Solid State Chem. **25**, 1 (1997).

[30]C. S. Johnson, M. F. Mansuetto, M. M. Thackeray, Y. Shao-Horn, and S. A. Hackney, J. Electrochem. Soc. **144**, 2279 (1997).

[31]Y. F. Shen, R. P. Zerger, R. N. DeGuzman, S. L. Suib, L. McCurdy, D. I. Potter, and C. L. O'Young, Science **260**, 511 (1993).

[32]S. Devaraj and N. Munichandraiah, J. Phys. Chem. C **112**, 4406 (2008).

[33]J. Kanamori, J. Phys. Chem. Solids **10**, 87 (1959).

[34]J. B. Goodenough, J. Phys. Chem. Solids **6**, 287 (1958).

[35]L. A. Fernandez, V. Martin-Mayor, S. Perez-Gaviro, A. Tarancon, and A. P. Young, Phys. Rev. B **80**, 024422 (2009).

[36]D. X. Viet and H. Kawamura, Phys. Rev. Lett. **102**, 027202 (2009).

[37]T. Hotta, S. Yunoki, M. Mayr, and E. Dagotto, Phys. Rev. B **60**, R15009 (1999).

[38]R. Kajimoto, H. Mochizuki, H. Yoshizawa, T. Kimura, and Y. Tokura, Physica B: Condensed Matter **312**, 760 (2002).

[39]N. Metropolis, A. W. Rosenbluth, M. N. Rosenbluth, and A. H. Teller, J. Chem. Phys. **21**, 1087 (1953).

[40]J. Villain, J. Phys. C: Solid State Phys. **10**, 1717 (1977).

[41]F. Shen, Y. Ding, J. Liu, Z. H. Han, J. Budnick, W. A. Hines, and S. L. Suib, J. Am. Chem. Soc. **127**, 6166 (2005).

[42]M. Hasenbusch, A. Pelissetto, and E. Vicari, Phys. Rev. B **78**, 214205 (2008).

[43]E. Marinari and G. Parisi, Europhys. Lett. **19**, 451 (1992).

[44]K. Hukushima and K. Nemoto, J. Phys. Soc. Jpn. **65**, 1604 (1996).

[45]A. Hartmann and H. Rieger, *Optimization Algorithms in Physics* (Wiley-VCH, Berlin, 2002).

[46]K. Binder, Z. Phys. B **43**, 119 (1981).

[47]R. N. Bhatt and A. P. Young, Phys. Rev. B **37**, 5606 (1988).

[48]N. Kawashima and A. P. Young, Phys. Rev. B **53**, R484 (1996).

[49]H. G. Ballesteros, A. Cruz, L. A. Fernandez, V. Martin-Mayor, J. Pech, J. J. Ruiz-Lorenzo, A. Tarancon, P. Tellez, C. L. Ullod, and C. Ungil, Phys. Rev. B **62**, 14237 (2000).

[50]T. Jörg, Phys. Rev. B **73**, 224431 (2006).